CARDIFF UNIVERSITY
PRIFYSGOL CAERDYDD

ORCA – Online Research @ Cardiff

This is an Open Access document downloaded from ORCA, Cardiff University's institutional repository:https://orca.cardiff.ac.uk/id/eprint/180358/

This is the author's version of a work that was submitted to / accepted for publication.

Citation for final published version:

Maccioni, Lucia, Brusaferri, Ludovica, Barzon, Leonardo, Schubert, Julia J., Nettis, Maria A., Cousins, Oliver, Rosenzweig, Ivana, Mizuno, Yuya, Vicente-Rodríguez, Marta, Singh, Nisha, Marques, Tiago R., Harrison, Neil A. , Fryer, Tim, Bullmore, Edward T., Cash, Diana, Mondelli, Valeria, Pariante, Carmine, Howes, Oliver, Turkheimer, Federico E., Loggia, Marco L. and Veronese, Mattia 2025. A novel blood-free analytical framework for the quantification of neuroinflammatory load from TSPO PET imaging. Journal of Cerebral Blood Flow & Metabolism 10.1177/0271678X251361261

Publishers page: http://dx.doi.org/10.1177/0271678X251361261

Please note:
Changes made as a result of publishing processes such as copy-editing, formatting and page numbers may not be reflected in this version. For the definitive version of this publication, please refer to the published source. You are advised to consult the publisher's version if you wish to cite this paper.

This version is being made available in accordance with publisher policies. See http://orca.cf.ac.uk/policies.html for usage policies. Copyright and moral rights for publications made available in ORCA are retained by the copyright holders.

A novel blood-free analytical framework for the quantification of neuroinflammatory load from TSPO PET Imaging

Supplementary Material

S1. Study participants and datasets

Dataset 1. KCL [^{11}C]PBR28 scans

A total of 118 dynamic [^{11}C]PBR28 PET and MR images collected both from healthy volunteers and patients were gathered from the KCL historical database (Age: 38±19 years; Sex: 84 male and 34 female; Genotype: 87 HABs and 31 MABs).

The dataset included 72 healthy controls (HC) with no family history of psychiatric or neurological conditions [1–3], 14 ultra-high-risk of psychosis (UHR) subjects (Bloomfield et al., 2016), 14 schizophrenia (SCZ) patients (Bloomfield et al., 2016), and 5 Alzheimer's disease (AD) patients [4] having test-retest scans with a mean inter-scan time of 82 ± 10.2 days, starting at the same time of the day, and with no significant difference between injected doses (test = 339.0 ± 4.6 MBq, retest = 350.8 ± 14.2 MBq, p = 0.154)). In addition, 7 subjects with schizophrenia (6 of which were included among the 14 SCZ patients) had 2 scans, before and immediately after receiving a 90mg oral dose of the TSPO antagonist XBD173, designed to reach between 66% and 77% of TSPO brain occupancy (XDB173 blocking before and XDB173 blocking after). The second scan was acquired approximately two years after the first acquisition - except for one subject for which the second scan was acquired only 1 week after - at a similar time of the day to the first one [5].

More details on participants and data acquisition can be found in the original references [1–5]. However, all acquisition protocols included an initial low-dose head computer tomography (CT) scan, acquired for attenuation and scatter correction, using a *Siemens Biograph™ TruePoint™ PET·CT scanner* (*Siemens Medical Systems, Germany*) and a dynamic PET scan after a bolus injection of [^{11}C]PBR28 (Injected Dose: 328.10 ± 32.79 MBq). The radiopharmaceutical preparation protocol was consistent in all the studies and was performed on-site immediately prior to use according to local guidelines and regulations.

For all the data, dynamic PET acquisition lasted 90 min and was binned into 26 frames (durations: 8×15s, 3×1min, 5×2min, 5×5min, 5×10min), except for the 10 AD dynamic image data which were collected over 60 min and binned into 23 frames (durations: 8×15s, 3×1min, 5×2min, 5×5min, 2×10min). PET images were reconstructed using filtered back projection, with a 5mm isotropic Gaussian smoothing, and corrected for random coincidences, attenuation, and scatter effects. T1w MR brain scan data were collected using a *Siemens 3T MR* scanner (either a *Siemens Tim Trio* or *Siemens MAGNETOM Verio*). In the case of AD patients, a clinical 1.5T T1w MR was carried out instead.

Dataset 2. MGH [^{11}C]PBR28 scans (scanner 1)

Data included a total of 46 [^{11}C]PBR28 scans acquired from 27 HCs and 19 patients affected by fibromyalgia (FM) (Age: 47 ± 13 years; Sex: 15 male and 31 female; Genotype: 30 HABs and 16 MABs). Data were gathered from previous studies [6–8]. In all studies, dynamic PET data acquisition was performed for 90 min after bolus injection of [^{11}C]PBR28 tracer (Injected Dose: 488.16 ± 54.99 MBq) with an integrated PET/MR scanner consisting of a dedicated brain avalanche photodiode-based PET scanner (Kolb et al., 2012) in the bore of a Siemens 3T Tim Trio MRI. Data were reconstructed using the 3D ordinary Poisson ordered subset expectation maximization (OP-OSEM) algorithm provided by the manufacturer and binned into 28 frames (duration: 8x10s, 3x20s, 2x30s, 1x1min, 1x2min, 1x3min, 8x5min, 4x10min). A multi-echo MPRAGE volume was acquired before tracer injection for anatomical localization and generation of attenuation correction maps using an in-house developed MR-based approach [9]. [^{11}C]PBR28 was produced in-house using a procedure modified from the literature [10].

Dataset 3. MGH [^{11}C]PBR28 scans (scanner 2)

Data included dynamic [^{11}C]PBR28 PET/MR images from 26 HCs (Age: 55 ± 15 years; Sex: 12 male and 14 female; Genotype: 13 HABs and 13 MABs) simultaneously collected on a *Siemens Biograph mMR* whole-body PET/MR scanner. Full details on the acquisition can be found in [11]. Dynamic PET data were acquired for 90 minutes after a bolus injection of [^{11}C]PBR28 (Injected Dose: 519.44 ± 63.04 MBq), binned into 28 frames (duration: 8x10s,

3x20s, 2x30s, 1x1min, 1x2min, 1x3min, 8x5min, 4x10min) and reconstructed using the Ordered Subset Expectation Maximisation (OSEM) with four iterations, 21 subsets, and a 3 mm Full Width Half Maximum (FWHM) Gaussian smoothing. As for dataset 2, [^{11}C]PBR28 tracer was produced in-house, and structural T1w images were used for the generation of attenuation correction maps [9].

Dataset 4. KCL [^{18}F]DPA-714 scans

Data included 57 [^{18}F]DPA-714 scans performed on 41 HCs and 16 subjects at increased risk of Alzheimer's disease (Age: 39 ± 19 years; Sex: 31 male and 26 female; Genotype: 37 HABs and 20 MABs). Specifically, the 16 patients at risk included 8 individuals who were carriers of the rare p.R47H genetic variant of the triggering receptor expressed on myeloid cells 2 immune receptor (TREM2) and 8 non-carriers with mild cognitive impairment (MCI) [12]. Dynamic data were collected on a SIEMENS Biograph mMR PET/MRI over 60 min after bolus injection of [^{18}F]DPA-714 (Injected Dose: 186.88 ± 10.00 MBq) and binned into 26 frames (1×1min, 8×15s, 3×1min, 5×2min, 9×5min). All participants underwent a CT head scan which was used for attenuation correction [13], and a T1w MRI on the *3T SIEMENS Biograph mMR*.

Dataset 5. KCL [^{11}C]-(*R*)-PK11195 scans

The dataset included 76 [^{11}C]-(*R*)-PK11195 PET/MR scans collected from 51 patients with mild-moderate depression (MD) and 25 age-matched HCs (Age: 37 ± 8 years; Sex: 26 male and 50 female) recruited as part of the BIODEP (Biomarkers in Depression) study (NIMA consortium; https://www.neuroimmunology.org.uk/biodep/). Details on inclusion criteria and data acquisition can be found in [14].

Dynamic PET data were acquired for 60 minutes after [^{11}C]-(*R*)-PK11195 injection (Injected Dose: 365.53 ± 50.89 MBq) on a *GE SIGNA* PET/MR (GE Healthcare, Waukesha, WI). Dynamic data were corrected for dead time, randoms, scatter, and decay directly on the scanner. Attenuation correction was performed with a multisubject atlas method [15,16] and improvements for the MRI brain coil component [17]. Dynamic sinograms were reconstructed using time-of-flight ordered subsets expectation maximization, with 6 iterations, 16 subsets, and no

smoothing, and binned into 17 frames (duration: 4x15s, 4x1min, 7x5min, 2x10min). All subjects underwent a high-resolution T1w brain MRI during PET acquisition.

S2. Image preprocessing

Data were analyzed using different combinations of in-house codes and neuroimaging analysis software including *Statistical Parametric Mapping 8* (*http://www.fil.ion.ucl.ac.uk/spm*), *FSL* (*http:// www.fsl.fmrib.ox.ac.uk/fsl*) and *MIAKAT™* (*http://www.miakat.org/MIAKAT2/ index.html*). All pipelines included a step of motion correction of the dynamic PET data, the computation of integral PET images, the derivation of brain tissue masks from structural MR images (performed using the *FreeSurfer* package), and the registration of brain and tissue masks, as well as of a neuroanatomical atlas – the *CIC* atlas version 2.0 [18] - to the subject's native PET space for the definition of ROIs. The CIC atlas was masked using a grey matter mask derived from the *FreeSurfer* parcellation image to exclude voxels belonging to white matter, cerebrospinal fluid, or outside the brain and then used for the computation of ROIs mean regional TACs for each subject. 116 out of 125 available ROIs from the CIC atlas, defining cortical, subcortical, and cerebellum regions, were retained for subsequent analyses.
Following the approach described in [19], an image-derived input function (IDIF) was extracted from the subjects' dynamic PET images via segmentation of blood voxels in the carotid siphons by intensity thresholding, and selection of the voxels with higher between dynamics correlation; mean blood TAC was thus computed and fitted with a tri-exponential model.
Regional tracer delivery rate (kinetic microparameter K_1) was finally computed for each ROI by application of a recently developed non-invasive and simplified methodologic framework consisting of fitting the first minutes (within 10 minutes) of the tracer kinetic in the tissue with a simplified compartmental model with 1 single irreversible compartment and IDIF. Further details on methodology and procedures for IDIF and K_1 estimation can be found in [19]. The choice of optimal fitting time window – allowing the satisfaction of model hypotheses - was based on dynamic data time resolution and the specific characteristics of tracer kinetics and metabolism. A four-minute window was adopted for [^{11}C]PBR28, while a five-minute window for the [^{18}F]DPA-714 and [^{11}C]-(*R*)-PK11195 scans.

S3. Features selection and model validation

The 72 healthy controls of Dataset 1 were divided into a training-validation set (80%, n=56) and a test set (20%, n=16) with a stratified split aiming at maintaining the same proportion of males and females, HABs and MABs, younger (under 30 years old) and older (over 30 years old) individuals between the two groups. All regressors were normalized to the [0 1] range with min-max normalization, with the minimum and maximum values computed from all the available data.

Feature selection was performed with the stepwise approach implemented in Matlab (function *stepwiseglm*), with model deviance adopted as a selection criterion. This step was repeated for 100 iterations using a bootstrap resampling approach and only features with a frequency of selection over 80% were kept as relevant features in the model. This approach was adopted to guarantee a more stable and robust selection of model covariates. Starting from the initial selection of model predictors (i.e. ROIs TACs samples at 1.25, 4.50, 13.50, 30, 50, and 75 minutes as well as ROIs K_1 and subjects' age, sex, genotype, and tracer dose over subjects' weight ratio), the resulting set of selected features included ROIs TAC samples at 1.25, 13.5 and 50 minutes, together with age, genotype, and the K_1 microparameter.

The performances of both the full model (with all original regressors) and the reduced model (with only the regressors that passed the stepwise selection) were evaluated on the test set. The ROC curve of method classification - starting from regional $\mathbf{p_{TSPO}}$ estimates - in discriminating tissues with different constitutive TSPO expressions was adopted for the evaluation of their performance. ROC curves reported in **Supplementary Figure 1a**, show good classification performances of TSPO tissue expression, in terms of sensitivity and specificity, of the logistic regression model. Comparable levels of sensitivity and specificity are reported for the full model (AUC=0.92, sensitivity=0.87, specificity=0.84) - including all the original predictors – and the reduced model (AUC=0.92, sensitivity=0.89, specificity=0.86) – with only the subset of predictors identified with the features selection.

Once the model set-up was optimized (i.e. the brain regions to adopt for model training and the subset of most informative predictors were selected), the logistic model was trained and tested on [^{11}C]PBR28 PET scans on 72, 27, and 26 HCs from three independent datasets (Dataset 1, Dataset 2 and Dataset 3). A random effect was included in the logistic regression model to account for differences in the acquisition between the three datasets, bringing to the definition of a hierarchical logistic regression model[20,21]. Again, the whole dataset was split into a training

and test set with a stratified division accounting for age, sex, genotype, and scanner. After parameters estimation on the training dataset, the model was applied to the test set, and model performances were evaluated in terms of classification accuracy, sensitivity, and specificity.
The hierarchical logistic regression model demonstrated good classification performances as shown by the ROC curves in **Supplementary Figure 1b**. Again, similar values of specificity and sensitivity are reported for the full (AUC=0.93, sensitivity=0.83, specificity=0.87) and reduced (AUC=0.92, sensitivity=0.85, specificity=0.89) models, confirming the reliability of adopting the subset of selected predictors.

S4. Model Covariates

To assess possible dependencies of ROIs $\mathbf{p_{TSPO}}$ from the set of covariates of interest, the distribution of cortex and cerebellum (CC) ROIs $\mathbf{p_{TSPO}}$ was compared between HABs and MABs, as well as between female and male volunteers; similarly, possible correlations between median value across CC ROIs of predicted $\mathbf{p_{TSPO}}$ for each subject and age or dose-over-weight ratio were investigated. Consistent with the set of covariates included in the model, post hoc analysis reveals no statistical differences in $\mathbf{p_{TSPO}}$ when comparing results for HABs and MABs, and no significant correlation with either age or dose-over-weight ratio.
Although sex was not retained as a significant predictor in the features selection step, post hoc analyses showed significantly lower values of CC ROIs $\mathbf{p_{TSPO}}$ for female than male HCs, thus highlighting sex as a possible factor affecting the level of TSPO in the brain. (**Supplementary Figure 2**). These results are in line with evidence from the literature reporting a dependency of TSPO density on sex, despite mixed results being shown so far, demonstrating increased or decreased TSPO expression in female compared to male individuals according to the type of quantification and metrics adopted[22–24]. Given the dependence of $\mathbf{p_{TSPO}}$ on sex, significant between-group differences in the proportion of males and females were thus checked for each case study under investigation. The chi-squared test found no significant differences between each pair of groups under study.

Supplementary Tables

Supplementary Table 1. Cross-sectional analyses - [^{11}C]PBR28

Groups	Number	Age (mean±std)	Sex (#M , #F)	Genotype (#HAB, #MAB)	Dataset
HC	13	27 ± 6	9 , 4	9 , 4	Dataset 1
UHR	14	24 ± 5	7 , 7	7 , 7	
HC	13	46 ± 14	10 , 3	13 , 0	Dataset 1
SCZ	14	47 ± 9	11 , 3	12 , 2	
BASELINE	7	46 ± 11	7 , 0	7 , 0	Dataset 1
Post XBD173	7	48 ± 11	7 , 0	7 , 0	
HC	72	32 ± 13	50 , 22	50 , 22	Dataset 1
AD	10	82 ± 4	8 , 2	10 , 0	
HC	16	46 ± 14	2 , 14	10 , 6	Dataset 2
FM	19	48 ± 12	2 , 17	13 , 6	
AD TEST	5	82 ± 4	4 , 1	5 , 0	Dataset 1
AD RETEST	5	82 ± 4	4 , 1	5 , 0	

HC=healthy control; UHR=ultra-high risk of psychosis; SCZ=schizophrenia; AD=Alzheimer's disease; FM=fibromyalgia; m=mean; std=standard deviation; HAB=high affinity binding; MAB=mixed affinity binding; M=males; F=females

Supplementary Table 2. Cross-sectional analyses - [^{18}F]DPA-714 and [^{11}C]-(*R*)-PK11195

Groups	Number	Age (mean±std)	Sex (#M, #F)	Genotype (#HAB, #MAB)	Dataset
MCI	8	70 ± 6	6 , 2	3 , 5	Dataset 4
TREM2	8	64 ± 4	3 , 5	4 , 4	
HC	25	37 ± 8	11 , 14	/	Dataset 5
MD	51	36 ± 7	15 , 36	/	

HC=healthy control; TREM2=TREM2 p.R47H carriers; MCI=mild cognitive impairment; MD=mild depressive disorders; m=mean; std=standard deviation; HAB=high affinity binding; MAB=mixed affinity binding; M=males; F=females.

Supplementary Table 3: Comparison of between-groups changes in $\mathbf{p_{TSPO}}$ and previous evidence of alterations in neuroinflammatory load with standard quantification

Case study	Findings from previous literature		Findings from p_{TSPO}
Ultra-high risk of psychosis	*2TCM1K DVR* [34] *	▪ total GM: γ = 1.2 ▪ frontal lobe: γ = 0.9 ▪ temporal lobe: γ = 0.8	▪ CC ROIs: γ = 0.5 ▪ frontal lobe: γ = 0.6 ▪ temporal lobe: γ = 0.4
Schizophrenia	*2TCM1K DVR* [34] *	▪ total GM: γ =1.8 ▪ frontal lobe: γ =1.2 ▪ temporal lobe: γ =1.4	▪ CC ROIs: γ =1.0 ▪ frontal lobe: γ =1.2 ▪ temporal lobe: γ = 0.6
Blocking study	*2TCM1K* V_T [37]	▪ total GM: γ = -1.9	▪ CC ROIs: γ =-1.3
Alzheimer's disease	*2TCM* V_T / f_p [12] *	▪ prefrontal: γ =1.0 ▪ inferior parietal: γ =1.5 ▪ superior temporal: γ =1.1 ▪ middle-inferior temporal: γ = 1.4 ▪ occipital: γ = 1.0	▪ CC ROIs: γ = -1.2 ▪ frontal lobe: γ = 1.5 ▪ parietal lobe: γ = 1.2 ▪ temporal lobe: γ = 0.7 ▪ occipital lobe: γ = 2.0
Fibromyalgia	$SUVr_{33\text{-}63}$ [36]	▪ frontal lobe: average γ = 0.8±0.2 ▪ parietal lobe: average γ = 1.3 ± 0.7	▪ frontal lobe: γ = 0.5 ▪ parietal lobe: γ = 0.4
Test-Retest	$SUV_{40\text{-}60}$ [35]	▪ whole brain: ICC= 0.94	▪ CC ROIs: average ICC = 0.88 [0.70 0.95]

2TCM = two reversible compartment model; *2TCM1K* = two reversible compartment model with vascular compartment; *DVR* = distribution volume ratio; V_T = volume of distribution; f_p= plasma free fraction; *SUV* = standardized uptake value; $SUV_{40\text{-}60}$ = average SUV between 40 and 60 minutes after tracer injection; $SUVr_{33\text{-}63}$ = average SUV ratio between 33 and 66 minutes after tracer injection; γ = non-parametric Cohen's d-consistent effect size (average γ reported as mean ± standard deviation); ICC= intraclass correlation coefficient (average ICC reported as median [interquartile range]); ROI= region of interest; CC ROIs= cerebellum and brain cortex ROIs (used here as proxy for cortical/total GM). * γ derived from original Cohen's d effect size, as γ converges to Cohen's d when comparing normal distributions.

Supplementary Figures

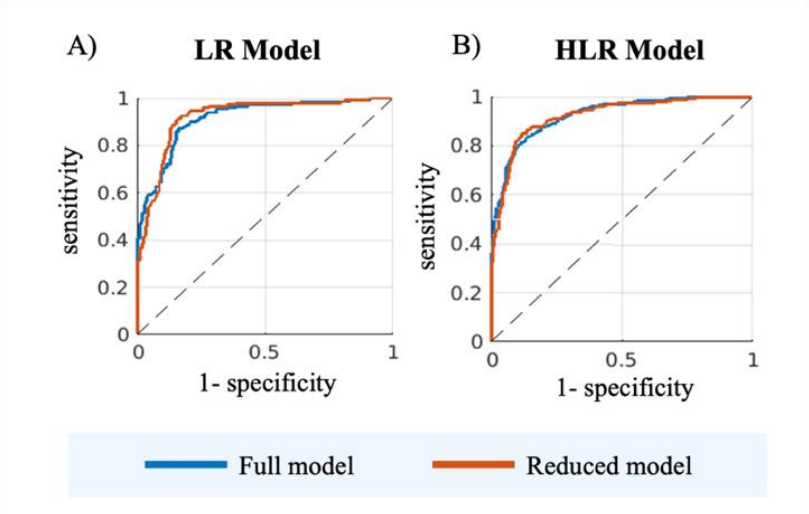

Supplementary Figure 1. Model Validation on [^{11}C]PBR28 data
The figure reports the ROC curve indicating the sensitivity and specificity of model classification for the logistic regression model (panel A) and the hierarchical logistic regression model (panel B).

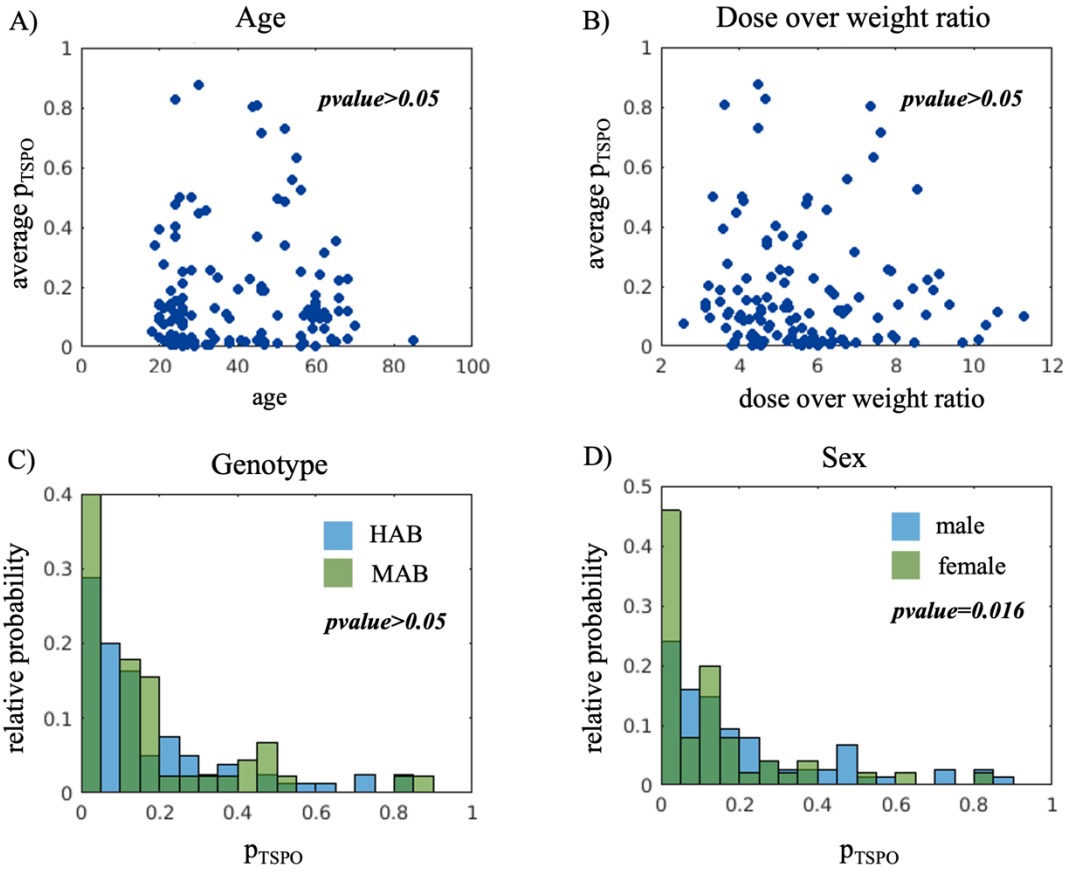

Supplementary Figure 2. Effect of age, sex, genotype, and dose-over-weight ratio on p_{TSPO} estimation

Panels A and B show the lack of a significant correlation between subjects' average (across CC-ROIs) p_{TSPO} with either age or dose over-weight ratio; panel C shows no statistical difference when comparing CC ROIs p_{TSPO} results of HAB and MAB groups; panel D shows a statistically significant difference when comparing CC ROIs p_{TSPO} between female and male subjects. Age and genotype were included as model covariates while sex and dose-over-weight were excluded from model predictors with the feature selection step; dose-over-wight ratio information is still adopted in the model for the normalization of TACs into SUV.

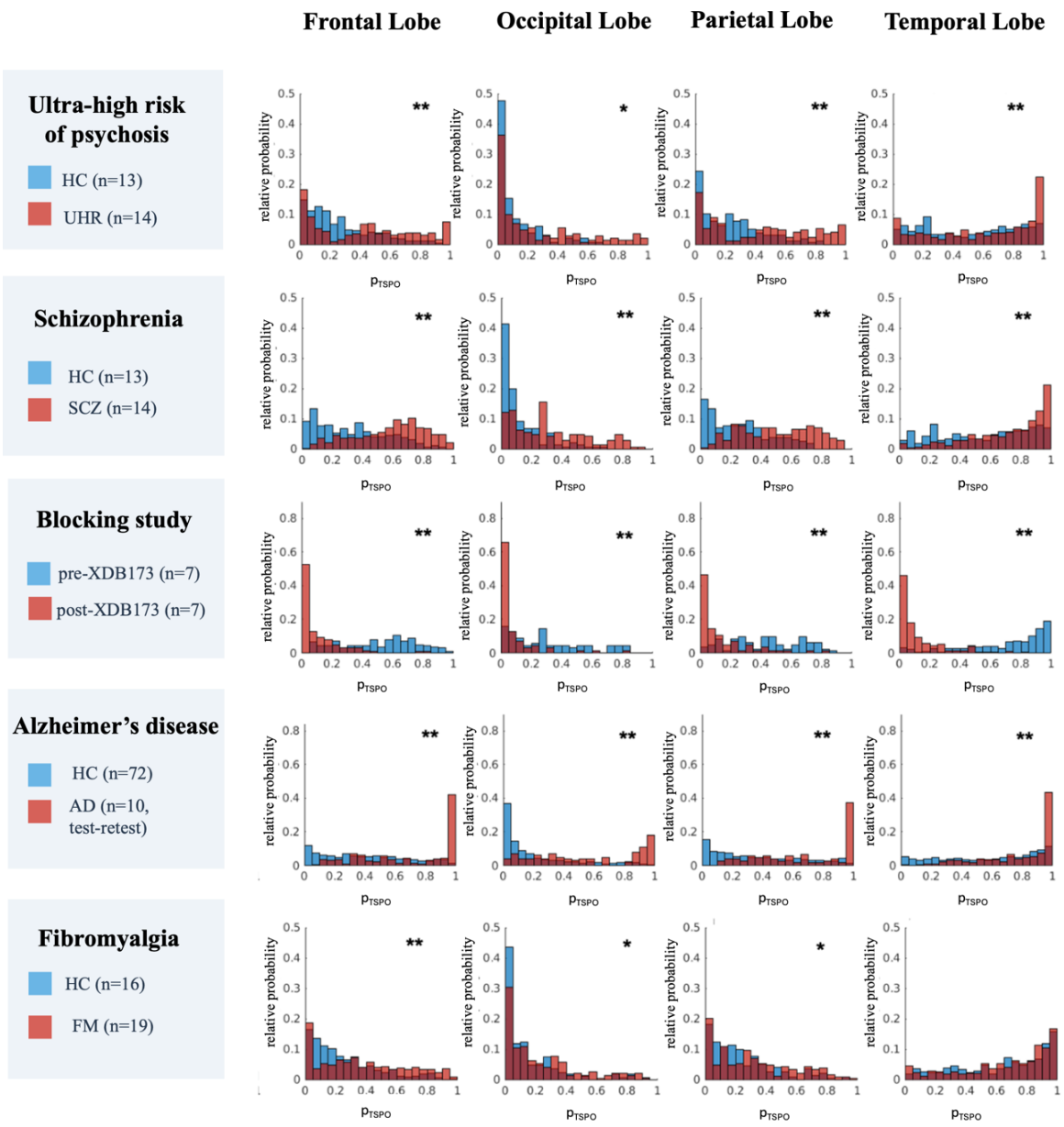

Supplementary Figure 3. Cross-sectional analysis – Comparison of ROIs p_{TSPO} relative probability for each lobe

Each panel shows, for each study under investigation, the comparison of the group relative probability of ROIs p_{TSPO} for four brain anatomical lobes (frontal, occipital, parietal and temporal) [HC=healthy controls; UHR=ultra-high risk of psychosis; SCZ=schizophrenia; AD=Alzheimer's disease; FM=fibromyalgia; * Wilcoxon test pvalue<0.05; ** Wilcoxon test pvalue<0.0001]

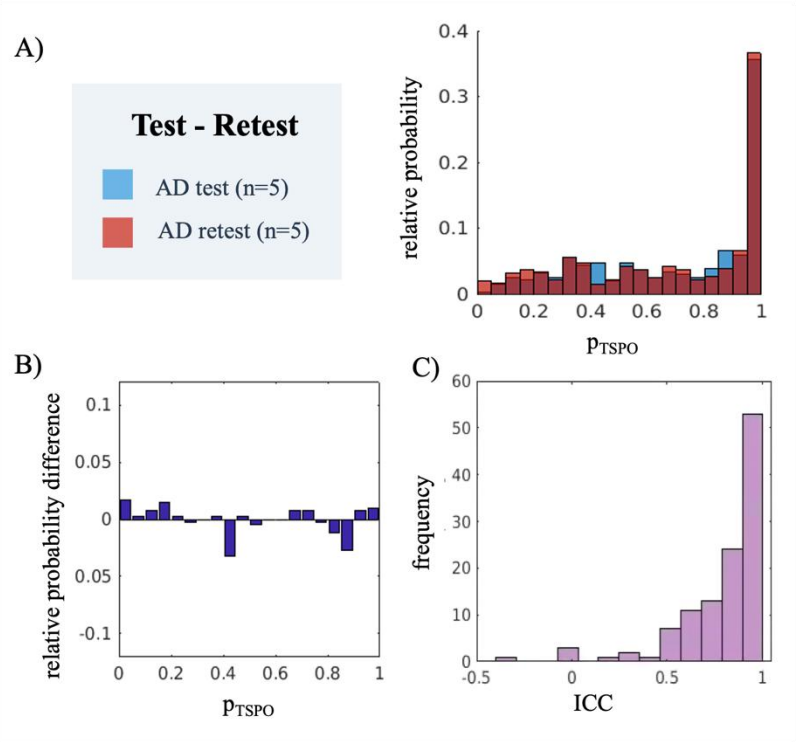

Supplementary Figure 4. Reproducibility analysis
The figure shows the results of reproducibility analysis on test-retest scans on Alzheimer's disease patients (AD): panel A shows a comparison of the group relative probability of CC ROIs $\mathbf{p_{TSPO}}$; in panel B the difference between the two relative probabilities is represented; panel C shows a histogram of CC ROIs ICC values [ICC=intraclass correlation coefficient].

References

1. Bloomfield PS, Selvaraj S, Veronese M, et al. Microglial Activity in People at Ultra High Risk of Psychosis and in Schizophrenia: An [^{11} C]PBR28 PET Brain Imaging Study. *AJP* 2016; 173: 44–52.

2. Dahoun T, Calcia MA, Veronese M, et al. The association of psychosocial risk factors for mental health with a brain marker altered by inflammation: A translocator protein (TSPO) PET imaging study. *Brain, Behavior, and Immunity* 2019; 80: 742–750.

3. Nettis MA, Veronese M, Nikkheslat N, et al. PET imaging shows no changes in TSPO brain density after IFN-α immune challenge in healthy human volunteers. *Transl Psychiatry* 2020; 10: 89.

4. Nair A, Veronese M, Xu X, et al. Test-retest analysis of a non-invasive method of quantifying [(11)C]-PBR28 binding in Alzheimer's disease. *EJNMMI Res* 2016; 6: 72.

5. Veronese M, Reis Marques T, Bloomfield PS, et al. Kinetic modelling of [^{11} C]PBR28 for 18 kDa translocator protein PET data: A validation study of vascular modelling in the brain using XBD173 and tissue analysis. *J Cereb Blood Flow Metab* 2018; 38: 1227–1242.

6. Albrecht DS, Forsberg A, Sandström A, et al. Brain glial activation in fibromyalgia – A multi-site positron emission tomography investigation. *Brain, Behavior, and Immunity* 2019; 75: 72–83.

7. Alshelh Z, Albrecht DS, Bergan C, et al. In-vivo imaging of neuroinflammation in veterans with Gulf War illness. *Brain, Behavior, and Immunity* 2020; 87: 498–507.

8. Torrado-Carvajal A, Toschi N, Albrecht DS, et al. Thalamic neuroinflammation as a reproducible and discriminating signature for chronic low back pain. *Pain* 2021; 162: 1241–1249.

9. Izquierdo-Garcia D, Hansen AE, Förster S, et al. An SPM8-Based Approach for Attenuation Correction Combining Segmentation and Nonrigid Template Formation: Application to Simultaneous PET/MR Brain Imaging. *J Nucl Med* 2014; 55: 1825–1830.

10. Imaizumi M, Kim H-J, Zoghbi SS, et al. PET imaging with [11C]PBR28 can localize and quantify upregulated peripheral benzodiazepine receptors associated with cerebral ischemia in rat. *Neuroscience Letters* 2007; 411: 200–205.

11. Morrissey EJ, Alshelh Z, Knight PC, et al. Assessing the potential anti-neuroinflammatory effect of minocycline in chronic low back pain: Protocol for a randomized, double-blind, placebo-controlled trial. *Contemporary Clinical Trials* 2023; 126: 107087.

12. Cousins O, Schubert JJ, Chandra A, et al. Microglial activation, tau and amyloid deposition in TREM2 p.R47H carriers and mild cognitive impairment patients: a multi-

modal/multi-tracer PET/MRI imaging study with influenza vaccine immune challenge. *Journal of Neuroinflammation* 2023; 20: 272.

13. Mackewn JE, Stirling J, Jeljeli S, et al. Practical issues and limitations of brain attenuation correction on a simultaneous PET-MR scanner. *EJNMMI Physics* 2020; 7: 24.

14. Schubert J, Veronese M, Fryer TD, et al. A Modest Increase in 11C-PK11195-Positron Emission Tomography TSPO Binding in Depression Is Not Associated With Serum C-Reactive Protein or Body Mass Index. *Biol Psychiatry Cogn Neurosci Neuroimaging* 2021; 6: 716–724.

15. Burgos N, Cardoso MJ, Thielemans K, et al. Attenuation correction synthesis for hybrid PET-MR scanners: Application to brain studies. *IEEE Transactions on Medical Imaging* 2014; 33: 2332–2341.

16. Prados Carrasco F, Cardoso MJ, Burgos N, et al. NiftyWeb: web based platform for image processing on the cloud. *In: Proceedings of the 24th Scientific Meeting and Exhibition of the International Society for Magnetic Resonance in Medicine (ISMRM). International Society for Magnetic Resonance in Medicine (ISMRM): Singapore. (2016)*; 24. Epub ahead of print 13 May 2016. DOI: 10/1/Submit-niftyweb.pdf.

17. Manavaki R, Hong YT, Fryer TD. Brain MRI Coil Attenuation Map Processing for the GE SIGNA PET/MR: Impact on PET Image Quantification and Uniformity. In: *2019 IEEE Nuclear Science Symposium and Medical Imaging Conference (NSS/MIC)*, pp. 1–2.

18. Tziortzi AC, Searle GE, Tzimopoulou S, et al. Imaging dopamine receptors in humans with [11C]-(+)-PHNO: Dissection of D3 signal and anatomy. *NeuroImage* 2011; 54: 264–277.

19. Maccioni L, Michelle CM, Brusaferri L, et al. A blood-free modeling approach for the quantification of the blood-to-brain tracer exchange in TSPO PET imaging. *Front Neurosci*; 18. Epub ahead of print 22 July 2024. DOI: 10.3389/fnins.2024.1395769.

20. Bryk AS, Raudenbush SW. *Hierarchical linear models: Applications and data analysis methods*. Thousand Oaks, CA, US: Sage Publications, Inc, 1992.

21. Degenholtz HB, Bhatnagar M. Introduction to Hierarchical Modeling. *Journal of Palliative Medicine* 2009; 12: 631–638.

22. Laaksonen S, Saraste M, Nylund M, et al. Sex-driven variability in TSPO-expressing microglia in MS patients and healthy individuals. *Front Neurol* 2024; 15: 1352116.

23. Peyronneau M, Kuhnast B, Nguyen D-L, et al. [18F]DPA-714: Effect of co-medications, age, sex, BMI and TSPO polymorphism on the human plasma input function. *Eur J Nucl Med Mol Imaging* 2023; 50: 3251–3264.

24. Tuisku J, Plavén-Sigray P, Gaiser EC, et al. Effects of age, BMI and sex on the glial cell marker TSPO - a multicentre [11C]PBR28 HRRT PET study. *Eur J Nucl Med Mol Imaging* 2019; 46: 2329–2338.